Eighth to sixteenth virial coefficients of the Lennard-Jones model

Chao Feng, Andrew J. Schultz, Vipin Chaudhary, and David A. Kofke

Citation: The Journal of Chemical Physics **143**, 044504 (2015); doi: 10.1063/1.4927339
View online: http://dx.doi.org/10.1063/1.4927339
View Table of Contents: http://scitation.aip.org/content/aip/journal/jcp/143/4?ver=pdfcov
Published by the AIP Publishing

Eighth to sixteenth virial coefficients of the Lennard-Jones model

Chao Feng,[1,a)] Andrew J. Schultz,[2,b)] Vipin Chaudhary,[1,c)] and David A. Kofke[2,d)]
[1]*Department of Computer Science and Engineering, University at Buffalo, The State University of New York, Buffalo, New York 14260, USA*
[2]*Department of Chemical and Biological Engineering, University at Buffalo, The State University of New York, Buffalo, New York 14260, USA*

(Received 12 June 2015; accepted 14 July 2015; published online 24 July 2015)

We calculated virial coefficients B_N, $8 \le N \le 16$, of the Lennard-Jones (LJ) model using both the Mayer-sampling Monte Carlo method and direct generation of configurations, with Wheatley's algorithm for summation of clusters. For $N = 8$, 24 values are reported, and for $N = 9$, 12 values are reported, both for temperatures T in the range $0.6 \le T \le 40.0$ (in LJ units). For each N in $10 \le N \le 16$, one to four values are reported for $0.6 \le T \le 0.9$. An approximate functional form for the temperature dependence of B_N was developed, and fits of LJ $B_N(T)$ based on this form are presented for each coefficient, $4 \le N \le 9$, using new and previously reported data. © *2015 AIP Publishing LLC.* [http://dx.doi.org/10.1063/1.4927339]

I. INTRODUCTION

The virial equation of state (VEOS) is a density expansion with respect to an ideal-gas reference that builds a bridge between molecular and macro-scale descriptions of fluid-phase behavior.[1] It can be expressed as follows, where we write the compressibility factor Z in powers of the number density ρ,

$$Z \equiv \beta P/\rho = 1 + B_2(T)\rho + B_3(T)\rho^2 + \cdots + B_n(T)\rho^{n-1} + \cdots. \quad (1)$$

Here, $\beta = 1/k_B T$ with T the absolute temperature and k_B Boltzmann's constant, P is the pressure, and B_N is the (temperature-dependent) Nth virial coefficient. Although most often written in the context of the pressure-density relation, the VEOS framework can describe a much broader range of behaviors while accommodating a variety of complicating phenomena, such as inhomogeneities,[2–4] non-pairwise interactions,[5–7] electrostatics,[8] and nuclear quantum effects.[9–11]

An appealing feature of the VEOS is that it can provide a description of the bulk-phase behavior in the thermodynamic limit, through consideration of the interactions of just a few molecules. This positions it as a route to derive thermodynamic behavior from first-principles methods.[12] The prospects of accomplishing this are limited by issues related to the convergence of the virial series, and progress in understanding these issues can benefit from knowledge of the behavior of the virial coefficients with increasing order. Moreover, interesting questions have resurfaced recently concerning how the virial series relates to condensation,[13–15] and these may be better addressed with knowledge of high-order coefficients.

Unfortunately, the difficulty[16] of computing the coefficient B_N—the amount of computational effort required to evaluate it to a given precision—increases exponentially[17,18] with N, and consequently the known virial coefficients do not reach to very high order. For a long time, data were available only for very simple models, and even for those cases it was unusual to find values of B_N for $N > 5$ (the hard-sphere (HS) model being a notable exception). The advent of Mayer-sampling Monte Carlo[19] (MSMC) made it possible to evaluate coefficients for much more complex models, but calculations are still practically restricted to $N \le \sim 8$. Thus, we now have, for example, values of B_N for water using models both non-polarizable ($N \le 6$)[20,21] and polarizable ($N \le 5$);[5,6] short n-alkanes ($N \le 6$), and longer chains of up to 20 carbon atoms ($N \le 4$);[22] and helium-4 using both a semiclassical treatment ($N \le 5$)[23] and a full quantum Boltzmann representation based on path-integral methods ($N \le 4$),[11] both approaches using *ab initio* based 2- and 3-body interactions for the helium atoms. Other examples can be cited, reporting B_N for N in the range of about 3 to 8.

Another breakthrough in methodology was offered recently by Wheatley.[17] His algorithm, reviewed below, greatly improves the efficiency of calculations for $N \ge 6$ and makes possible calculations beyond the $N = 8$ "barrier." Calculation of virial coefficients from a molecular model entails evaluation of a high-dimensional integral, and Wheatley's algorithm focuses on efficient evaluation of the integrand. It thus complements MSMC, which is focused on sampling of configurations and defining averages that yield the integral reliably and efficiently. Wheatley's algorithm scales exponentially with N in time and memory, which is much better (for larger N) than the scaling obtained by the direct sum of clusters that defines the integrand. Application of the method has so far focused on simple models, but the technique is in no way restricted to such cases. Virial coefficients have been computed up to $N = 12$ for the three-dimensional HS model;[17,18,24] Zhang and Pettitt[24] have computed very high-order coefficients for HS in high dimensions using a combination of Wheatley's algorithm and other methods; and Wheatley used his method to compute B_N for $N = 5$ to 10 for a soft-sphere model.

[a)]chaofeng@buffalo.edu
[b)]ajs42@buffalo.edu
[c)]vipin@buffalo.edu
[d)]kofke@buffalo.edu

The present work focuses on the Lennard-Jones (LJ) model, whereby the spherically symmetric pair potential $u(r)$ for two LJ particles at a separation r is

$$u(r) = 4\epsilon_{\mathrm{LJ}}\left[\left(\frac{\sigma_{\mathrm{LJ}}}{r}\right)^{12} - \left(\frac{\sigma_{\mathrm{LJ}}}{r}\right)^{6}\right], \tag{2}$$

where σ_{LJ} is the diameter of the atom and ϵ_{LJ} is the depth of the attractive energy well. Henceforth, we adopt units such that σ_{LJ} and $\epsilon_{\mathrm{LJ}}/k_{\mathrm{B}}$ are both unity (LJ units). It is worth emphasizing that our calculations employ the full potential, and no truncation is applied either explicitly or implicitly. Such truncation would affect the virial coefficients, as has been shown in other studies.[25]

Evaluation of virial coefficients for the LJ model has a long history. Barker *et al.*[26] described a numerical method for evaluating virial coefficients of the LJ model and reported values up to B_5. Henderson and Oden[27] calculated coefficients up to B_4 for many temperatures. Kim *et al.*[28] then provided more precise results than Barker. Sun and Teja[29] calculated coefficients from $N = 2$ to 5 for many temperatures. Dyer *et al.*[30] applied Fourier methods and direct quadrature to obtain very precise values of B_4. In proposing MSMC, Singh and Kofke[19] demonstrated the method for LJ virial coefficients from B_2 to B_6. Schultz and Kofke[31] then calculated coefficients for B_7 and B_8, while reporting improved values for $N = 4$, 5, and 6. Later, Schultz *et al.*[32] reported values of B_6, B_7, and B_8 with better precision and for more temperatures.

The present work is related to our recent study[33] examining the performance of graphics processing units (GPUs) to calculate the 8th, 9th, and 10th virial coefficients of the LJ model by MSMC and Wheatley's algorithm. The focus of that study was on the performance of the algorithm on GPUs, and on presenting a mixed-precision approach to address potential complications related to precision loss when using Wheatley's algorithm. In the course of that work, we calculated virial coefficients up to B_{10}, but we did not report them. However, we noticed that the relative difficulty[16] of the calculations decreased sharply with decreasing temperature, such that B_{10} at $T = 0.6$ (LJ units) could be evaluated with less relative difficulty than B_8 at $T = 1.0$. This has prompted us to investigate higher-order coefficients at lower temperatures, so as to gather data that can be used to study convergence of the virial series.

Accordingly, in this work, we report more precise values for B_8 and new values for B_8 to B_{16} for the LJ potential. The higher-order coefficients are increasingly focused on low temperatures, where the calculations are most feasible. Our attention is on detailing these calculations and presenting the results. In Section II, we describe the models and techniques, and in Section III, we present and discuss our results before concluding in Section IV.

II. METHODS

The Nth order classical virial coefficient B_N is formally expressed as a multi-dimensional integral over the coordinates of N particles. Specifically, for a spherically symmetric potential,[34]

$$B_N = \frac{1-N}{N!}\int \cdots \int f_B(\mathbf{r}^N) d\mathbf{r}_{12} \ldots d\mathbf{r}_{1N}, \tag{3}$$

where $d\mathbf{r}_{12} \ldots d\mathbf{r}_{1N}$ indicates integration over the positions of $N-1$ molecules with respect to the position of molecule 1, which defines the origin. Here, $f_B(\mathbf{r}^N)$ is the sum of biconnected graphs on N vertices, with each vertex corresponding to a molecule. For a pairwise-additive potential, each biconnected graph corresponds to a product of Mayer functions,

$$f_B(\mathbf{r}^N) = \sum_G \prod_{ij \in G} f_{ij}. \tag{4}$$

The Mayer function f_{ij}, which is the basic component of the integrand, is a function of distance (r_{ij}) between vertices labeled i and j in the configuration $\mathbf{r}^N$. It is given in terms of the pair potential $u(r_{ij})$ by

$$f_{ij} = e^{-\beta u(r_{ij})} - 1. \tag{5}$$

A. Overlap sampling

Monte Carlo (MC) methods for evaluation of multi-dimensional integrals (such as that in Eq. (3)) are based on calculation of the ratio of the target integral to a known reference integral, one defined over the same set of coordinates. For an accurate result, it is essential that the MC sampling allows for exploration of all configurations of importance to both integrals.[35] This is accomplished most reliably via separate processes, each performing importance sampling on the respective integrals. The appropriate way to combine these separate averages was given by Bennett[36] and adapted by us[20,21] for calculation of virial coefficients,

$$B_N = B_{N,0}\frac{\langle \gamma/\pi \rangle_\pi / \langle \gamma_{OS}/\pi \rangle_\pi}{\langle \gamma_0/\pi_0 \rangle_{\pi_0} / \langle \gamma_{OS}/\pi_0 \rangle_{\pi_0}}, \tag{6}$$

where the angle brackets specify an ensemble average weighted by π or π_0, as indicated, and the subscript 0 indicates a quantity corresponding to the reference integral. Here, γ is the integrand of the target integral (which in the present case is f_B), and the reference integral $B_{N,0}$ is

$$B_{N,0} = \int \cdots \int \gamma_0(\mathbf{r}^N) d\mathbf{r}_{12} \ldots d\mathbf{r}_{1N}, \tag{7}$$

which gives $B_{N,0}$ in terms of the reference-system integrand γ_0. The choice of the reference is discussed in Sec. II B. There are four averages appearing in Eq. (6). In what follows, we will refer to $\langle \gamma/\pi \rangle_\pi$ as the "target-system average," and $\langle \gamma_{OS}/\pi \rangle_\pi$ as the "target-system overlap average." The corresponding terms in the denominator of Eq. (6) will be called the "reference-system average" and "reference-system overlap average," respectively.

The integrand γ can exhibit negative values, so we cannot use it directly for the importance-sampling weight, but must instead use its absolute value: $\pi = |\gamma|$ (a consequence of this is that Eq. (6) gives B_N in terms of a ratio of ratios, rather than via a simple ratio); likewise, $\pi_0 = |\gamma_0|$. With this choice of sampling weight, the target- and reference-system averages are both taken over quantities that can equal only ±1.

Finally, γ_{OS} is the overlap function given by

$$\gamma_{OS} = \frac{\pi\pi_0}{\alpha\pi_0 + \pi}, \tag{8}$$

where α is a parameter selected to optimize the convergence of the calculation.[21] Additional optimization is achieved by distributing the computational effort expended on the target versus reference systems such that their marginal contribution to the stochastic error of B_N is equalized.

B. Choice of reference and generation of configurations

For the target system, the importance sampling required by Eq. (6) can be accomplished using MSMC.[19] Such a simulation is performed in an infinite volume without any periodic boundaries, and no cutoff is applied to the potential. Configurations of particles are generated as a Markov chain via a Metropolis Monte Carlo process[37] to sample π, which has the effect of naturally confining the molecules to the vicinity of the origin, where molecule 1 is fixed.

The reference system is defined by γ_0, which in turn can be defined via a graph or sum of graphs, and a reference potential $u_0(r)$. The choice of γ_0 considers its similarity to the target, γ, how easily it can be importance-sampled, and availability of $B_{N,0}$. Common practice selects the HS potential for u_0, and we did that as well. From here, we employed two different choices of the graphs defining γ_0. In the first choice, which we used for $N = 8$ and 9, it is equal to graph sum for f_B: $\gamma_0 = f_B^{\mathrm{HS}}$; in the second, which we used for $N \geq 10$, it is a single graph G_C formed by joining N vertices with $N - 1$ bonds to make a chain: $\gamma_0 = G_C^{\mathrm{HS}}$.

For $\gamma_0 = f_B^{\mathrm{HS}}$, we employed MSMC to importance-sample the reference. For increasing N, the expense required to evaluate γ_0 makes it desirable to use a rejection-free algorithm and to reduce the time required for samples in the Markov chain to decorrelate. Moreover, for $N > 11$, good values of $B_{N,0}$ are not available for $\gamma_0 = f_B^{\mathrm{HS}}$. For these reasons, we turned to $\gamma_0 = G_C^{\mathrm{HS}}$ for larger N. This reference is sufficiently simple that we could generate configurations directly, *de novo*, in proportion to their weight π_0: starting with sphere 1 at the origin, we placed a second sphere at random uniformly in the spherical region of diameter σ_0 centered on the first sphere. The third sphere was placed likewise about sphere 2, and so on until we finished with sphere N, placing it at a point of overlap with sphere $N - 1$. In general, the configuration that results is one that could have been generated instead with the spheres placed in a different sequence, and its probability of generation (its weight π_0) is proportional to the number of such sequences. This number must be evaluated for each configuration, because π_0 appears in the averages taken in the target and reference simulations, via Eq. (8). The algorithm we used to count the number of placement sequences consistent with a given configuration has been detailed elsewhere[18] and will not be repeated here. We will point out though that it is a central processing unit (CPU)-intensive calculation, similar to evaluation of f_B, so computational simplicity of γ_0 is not the primary benefit of using G_C^{HS}. Instead, the advantages are (1) it allows for direct generation of a series of uncorrelated importance-sampled configurations; (2) G_C^{HS} does not switch sign, so $\langle\gamma_0/\pi_0\rangle_{\pi_0} \equiv 1$; and (3) $B_{N,0}$ is trivial for this reference, and is equal to $(\frac{4}{3}\pi\sigma_0^3)^{N-1}$.

Direct generation of configurations without overlap-sampling the averages is the conventional method for evaluation of HS virial coefficients,[38] although in that case it is necessary to generate on additional graph structures to ensure that all relevant target-system configurations are accessible. In our calculation of HS virial coefficients,[18] we generated on trees and rings, as well, while Wheatley[17] used just a chain, but added a tail to the HS potential to enable a broader sample of configurations. In the present case, the chain structure for standard HS was sufficient because of our use of overlap sampling to compute the averages, which requires only that the directly generated configurations sample the reference system well.

C. Wheatley's algorithm

The conventional approach to evaluation of f_B is through summing of the terms of Eq. (4) directly. There are in total $2^{N(N-1)/2}$ possible graphs for N particles, which grows faster than exponentially with N, and the vast majority of these are biconnected and thus contribute to f_B.[18] As a consequence, it becomes impractical to calculate the integrand directly for $N > 8$.

As a remedy, Wheatley proposed an algorithm[17] that evaluates the integrand f_B in a less obvious, indirect manner. Wheatley's algorithm begins by calculating the sum of all $2^{N(N-1)/2}$ graphs, which is easily accomplished by computing the graph of N points with an $f + 1$ bond joining each pair of vertices. The desired sum is obtained from this by first subtracting contributions made by the disconnected graphs, leaving a sum of all connected graphs, and then subtracting from this the contributions made by graphs having articulation points (singly connected graphs). The final sum obtained is that for biconnected graphs only. A recursive approach is employed throughout.

The recursive nature of Wheatley's method introduces a potential problem with loss of precision for configurations where particles are far apart and f_B is near zero. Wheatley circumvented this problem for his soft-sphere calculations through a simple truncation scheme,[17] and we showed[33] that this scheme—in which f_B is set to zero for any configuration where it is calculated to be less than a threshold value—can be safely applied up to B_{10} for the LJ model using a 10^{-12} threshold. We used this same threshold in the present work and examined its suitability for calculations up to B_{16}.

D. Computational details

All calculations were based on the overlap-sampling averaging method detailed in Eqs. (6) to (8). A hard-sphere reference potential with diameter $\sigma_0 = 1.5$ was employed for all calculations (except as described below). For B_8 and B_9, we used $\gamma_0 = f_B^{\mathrm{HS}}$, and for B_{10} to B_{16}, we used $\gamma_0 = G_C^{\mathrm{HS}}$.

Many independent MSMC runs were performed for each temperature and each coefficient, and for each case the averages appearing in Eq. (6) were combined to compute

the reported B_N values. This parallelization was essential to completing the CPU-years of computational effort required to obtain the coefficients with good precision. In almost all cases, at least 80 such independent runs were performed, and in some cases as many as 5661 were used (more simulations were performed at temperatures near the critical temperature). Sampling of reference and target systems was completed independently, and the amount of sampling allotted to each was balanced to optimize the precision of the resulting B_N for a given total amount of sampling. Generally, the reference reached the desired precision with less sampling than the target system. Configurational averages were monitored through the course of the sampling process to guard against problems with ergodicity, wherein the system gets trapped in a single high-weight basin; such difficulties were observed only at temperatures below about $T \approx 0.2$, which are much lower than those reported here.

For B_8, each temperature totaled somewhere between 10 and 707.5×10^9 steps across all independent runs, requiring 11.9 to 815 CPU days of computational effort. Calculation of B_9 included 200 to 1500 simulations of 20 to 150×10^9 steps, ranging from 80.6 to 563.2 CPU days. For B_{10}, coefficients at four low temperatures were calculated, where 420×10^6 to 16.47×10^9 steps were performed with 5.6 to 216.5 CPU days. For B_{11}, we sampled 1161 to 6174×10^6 configurations, using 46.4 to 229.6 CPU days. For B_{12}, B_{13}, and B_{14}, coefficients at $T = 0.6$ and 0.7 were calculated at each order, where for B_{12} the steps were, respectively, 867 and 1716×10^6, using 98 and 200.3 CPU days; for B_{13}, 866 and 1289.6×10^6 steps using 305.9 and 448.6 CPU days; for B_{14}, 273 and 271.8×10^6 steps for each temperature spent 286.6 and 309.3 CPU days. For B_{15} and B_{16}, only the value at $T = 0.6$ was calculated, where 111.4×10^6 steps were used for B_{15} with 416.2 CPU days, and 66.4×10^6 steps ran for B_{16} using 808.9 CPU days.

For B_8 and B_9, $\gamma_0 = f_B^{\mathrm{HS}}$, and we used Wheatley's algorithm to calculate this quantity for each configuration of the reference and target simulations. While $\langle \gamma_0/\pi_0 \rangle_{\pi_0}$ is independent of temperature, $\langle \gamma_{\mathrm{OS}}/\pi_0 \rangle_{\pi_0}$ is not, so reference-system simulations had to be run at each temperature of interest. To improve the reference-system precision for B_9, we averaged $\langle \gamma_0/\pi_0 \rangle_{\pi_0}$ across all temperatures. The reduction in uncertainty obtained by combining these averages was especially useful for low temperatures, where the target system was easier to compute and precision of the reference calculations was limiting. With the use of $\gamma_0 = G_C^{\mathrm{HS}}$ for B_{10} and higher, we did not need to do this, as $\langle \gamma_0/\pi_0 \rangle_{\pi_0}$ is exactly unity.

The uncertainties on all calculations were computed from the uncertainties in the four averages appearing in Eq. (6), and propagating them to B_N while accounting for the correlation in the target- and reference-system averages, respectively. The required variances and covariances were computed from the multiple independent runs performed at each condition, as described above. For B_8 and B_9, we further broke up the runs into sub-block averages to generate more data to improve the precision of the variance. We did not do this for B_{10} to B_{16}, because the independent simulations were each too short to provide independent sub-blocks. All uncertainties are reported as one standard deviation of the mean (68% confidence limits).

Calculations were performed on Intel Xeon CPUs with speed ranging from 2.13 to 2.67 GHz and having 8 to 32 cores. The code was written in C. Random numbers were generated using the MT19937 implementation of the Mersenne Twister[39] pseudorandom number generator (PRNG). MT19937 was seeded at the beginning of each simulation with four 4-byte integers from the Linux kernel's /dev/urandom PRNG. When running with multiple threads, each thread had its own PRNG initialized with different seeds.

III. RESULTS AND DISCUSSION

A. Performance of calculation

The difficulty D is a measure that quantifies the computational effort needed to evaluate a stochastic average. It is defined[16] in terms of the CPU time t (excluding any time used for equilibration) required to obtain an average with uncertainty σ,

$$D \equiv t^{1/2}\sigma. \tag{9}$$

This quantity is asymptotically independent of t for a sufficiently large amount of sampling. It is of interest to examine the difficulty of the calculation of B_N as a function of temperature and coefficient order N. However, study of the absolute difficulty is not particularly worthwhile, because its behavior is dominated by the huge variation in the magnitude of the coefficients with T and N. A more useful comparison is found by working with the relative difficulty $\bar{D}$, which divides the uncertainty by a characteristic scale factor, which we choose here to be the magnitude of the coefficient itself. The relative difficulty is preferably expressed in terms of its logarithm, which we have called[16] the difficulty index, $\mathcal{D}_N$, thus defined for coefficient B_N,

$$\mathcal{D}_N \equiv \log_{10}(D_N/|B_N|), \tag{10}$$

where D_N is the difficulty for calculation of coefficient B_N, with a convention that t is given in units of seconds. Note that every unit increase in $\mathcal{D}_N$ corresponds to a two-order-of-magnitude increase in CPU time to achieve the same relative precision.

The difficulty index for the obtained virial coefficients is shown in Fig. 1. The plot shows first that, unsurprisingly, the relative difficulty increases with N; it also exhibits a sharp increase with T, which explains our focus on low-temperature calculations in this work. Beyond this, $\mathcal{D}_N$ peaks at intermediate temperatures, then drops and levels off with increasing T. The virial coefficients themselves go through zero in this vicinity, which has much to do with the increase in $\mathcal{D}_N$ over this range—the absolute difficulty D_N (not shown) does not exhibit any unusual behavior near T_c. It is worth noting that the trends in $\mathcal{D}_8$ and $\mathcal{D}_9$ differ from the others at low temperature. This is a consequence of the use of a different reference γ_0 for these coefficients, and it suggests that B_8 and B_9 could have been computed more efficiently using $\gamma_0 = G_C^{\mathrm{HS}}$, rather than f_B^{HS}.

We now turn to consideration of the choice of the hard-sphere diameter σ_0 that defined the reference system. In principle, the value of B_N computed according to Eq. (6) is

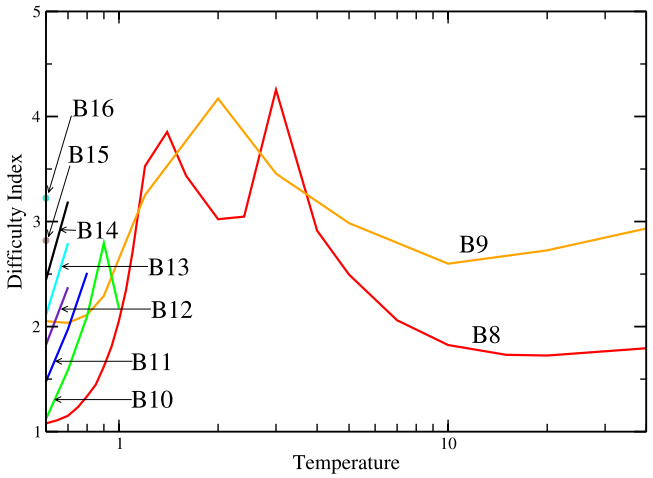

FIG. 1. Difficulty index $\mathcal{D}_N$ for calculation of the virial coefficients. For B_9, the value is based on the time for each calculation and does not reflect any economy obtained by exploiting the independence of $\langle \gamma_0/\pi_0 \rangle_{\pi_0}$ with temperature.

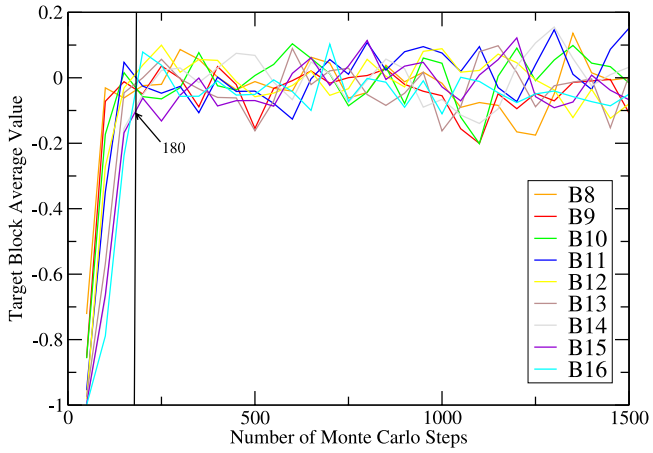

FIG. 3. Target block averages $\langle \gamma/\pi \rangle_\pi$ with increasing Monte Carlo steps, showing the initial equilibration phase of the simulation. Results are presented for $T = 0.6$.

independent of σ_0, but in practice this choice does affect the efficiency of the calculation. For the purpose of demonstrating how we selected σ_0, the relationship between σ_0 and relative uncertainty of the optimization parameter α is plotted in Fig. 2, taking B_8 and B_{10} at $T = 0.6$ as the examples. We observe that for both B_8 and B_{10}, the relative uncertainty of α reached a minimum at $\sigma_0 = 1.5$. When the relative uncertainty of α goes through a minimum, the relative uncertainty of the virial coefficient will also be a minimum. So we concluded that the best choice for σ_0 is 1.5, and we used this value for all other calculations. For higher temperatures, one can expect that smaller values of σ_0 would be optimal, considering the increasing relevance of the core region with increasing temperature. In our experience, such effects do not become significant until the temperature is increased substantially, say for $T > 10$; however, at such conditions, the reference averages add little to the overall computational cost, so the choice of σ_0 is not particularly important.

All calculations were begun from an initial configuration in which all particles were placed at the origin. It was necessary to perform a period of equilibration before the data collection began to allow the spheres to move to positions that were more appropriate to the importance-sampled average. To find the proper number of steps for equilibration, we examined block averages as a function of the number of MC trials, looking for the point where these averages ceased to exhibit a systematic trend. Fig. 3 shows that block averages of $\langle \gamma/\pi \rangle_\pi$ increased initially and then fluctuated within a stable range after 180 MC steps. In Fig. 4, we show that for $\langle \gamma_{OS}/\pi \rangle_\pi$ block averages, the number of steps required to reach a stable point increased with increasing order from B_8 to B_{16}: about 7800 MC steps were required for B_8, and up to 16 500 steps for B_{16}. The need for more equilibration steps was one of the reasons that the target system for high-order virial coefficients was more expensive to execute.

It is known that Wheatley's method can fail if the recursive calculation is not carried to sufficient precision.[17,33] The problem arises, in particular, for configurations where the atoms are distant from each other and their energy is small. In this circumstance, γ may be smaller than can be resolved by the precision used for the calculation, and effectively a lower bound is imposed on its magnitude. Although the failure may

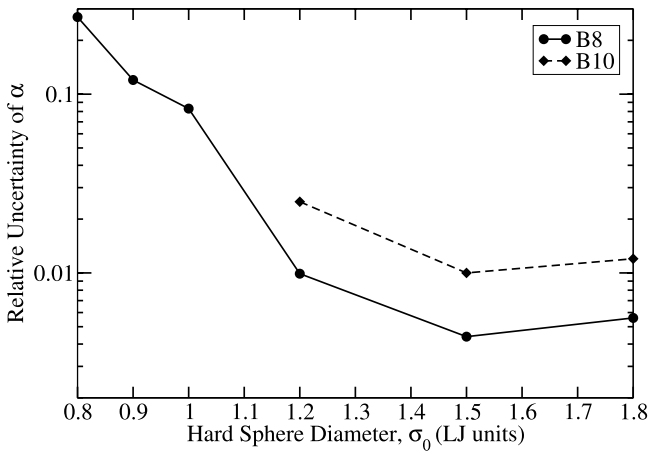

FIG. 2. The relationship between hard sphere diameter of the reference system (σ_0) and relative uncertainty of α (Eq. (8)), for $T = 0.6$.

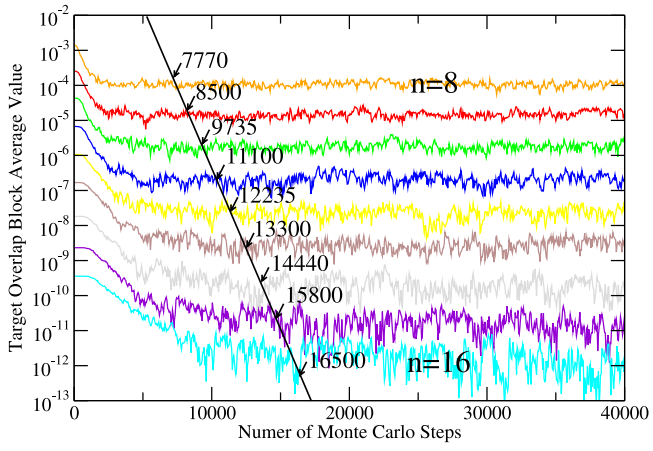

FIG. 4. Target overlap block averages $\langle \gamma_{OS}/\pi \rangle_\pi$ with increasing Monte Carlo steps, for $T = 0.6$. Traces are provided representing each virial-coefficient order examined in this work.

occur as only a rare event, its effect can be disproportionate, causing failure of the simulation. In some situations, the precision loss can lead to anomalously large contributions to the simulation averages, but with the use of overlap sampling for averaging, this mode of failure is less of an issue. Instead, here the primary concern is the effect on importance sampling—if the system enters a region of configuration space where the precision problem prevents accurate evaluation of weights, the landscape effectively becomes flat, and it is very unlikely that the Markov process will find its way back to the relevant configurations. Notably, γ_0 for the HS reference does not suffer from this problem, because all calculations of f_B^{HS} and G_C^{HS} are completed with integer arithmetic. So it is an issue only for the target-system sampling.

It has been found that a simple and effective remedy to the precision problem is to set f_B to zero when its computed magnitude falls below a pre-set lower bound.[17,33] In our previous work,[33] we compared the integrand calculated using the data type "double" (having 64 bits of precision) with that computed using "__float128" (having 128 bits), and showed that for B_6, B_8, and B_{10}, 10^{-12} is an appropriate truncation level. For values of f_B below this threshold, we observed significant differences between the 64- and 128-bit calculations, and above it we did not. We also performed 128-bit calculations to determine the contribution to the averages made by the configurations having f_B below the truncation level. We showed that their contribution was less than the uncertainty of the virial-coefficient averages that we computed, so no correction for the truncation was needed.[33]

Here, we extend this experiment up to B_{16}. Fig. 5 plots values of f_B computed using 64-bit arithmetic versus values for the same configurations computed using 128 bits. Any point falling significantly away from the line $y = x$ indicates an anomaly due to loss of precision. The figure shows that for B_{14} and B_{16}, many anomalous points lie above 10^{-12} as computed using 64 bits. This indicates that for these coefficients, we encountered configurations affected by the precision problem (when computed with 64 bits) that were not blocked by the truncation of f_B at 10^{-12}. The figure shows that instead 10^{-10} was an appropriate truncation for these higher coefficients. We in fact made this observation only after completing our calculations, having performed them using the 10^{-12} truncation. Nevertheless, we know that the problem did not taint our calculations because we never observed the expected mode of failure, in which the system gets lost in a low-precision landscape. This is understandable, because for the $N > 10$ low-temperature calculations, f_B was typically of order 10^{10}, and consequently there was effectively no chance that it would find its way into a configuration where it is 10^{-10} or smaller.

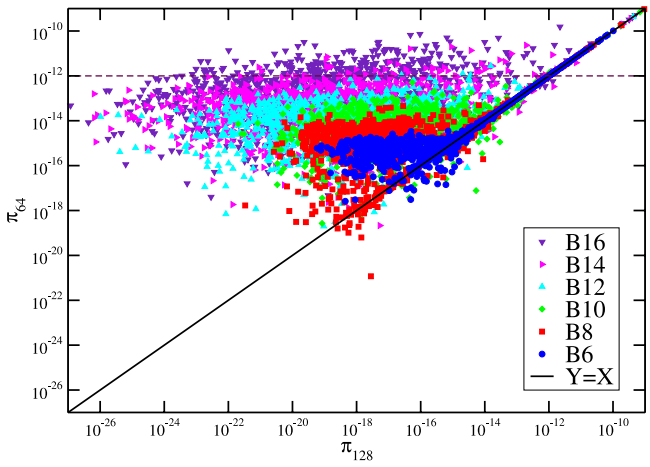

FIG. 5. Construction used to determine proper truncation for integrand value calculated using 64-bit arithmetic. x-axis is configuration weight as computed by 128-bit arithmetic, and y-axis is the same value computed using 64 bits. Points are values observed in configurations with weights falling in the plotted range, from simulations of the indicated coefficient. Solid black line is $y = x$.

TABLE I. Eighth virial coefficient of the Lennard-Jones model. All quantities given in LJ units.

T	B_8	B_8 (Ref. 32)
0.6	$-1.357(15) \times 10^{10}$	$-1.3(5) \times 10^{10}$
0.65	$-1.84(2) \times 10^{9}$	
0.7	$-3.03(4) \times 10^{8}$	
0.75	$-5.79(9) \times 10^{7}$	
0.8	$-1.30(3) \times 10^{7}$	$-1.48(19) \times 10^{7}$
0.85	$-3.11(4) \times 10^{6}$	
0.9	$-7.95(12) \times 10^{5}$	
0.95	$-2.18(4) \times 10^{5}$	
1.0	$-6.11(16) \times 10^{4}$	$-6.4(19) \times 10^{4}$
1.05	$-1.63(8) \times 10^{4}$	
1.1	$-3.7(3) \times 10^{3}$	
1.2	$-20(10) \times 10^{1}$	
1.4	18(16)	
1.6	13(5)	
2.0	5.4(8)	5(2)
2.4	1.3(3)	
3.0	−0.02(6)	
4.0	−0.09(2)	
5.0	$-8.7(7) \times 10^{-2}$	$-10.1(8) \times 10^{-2}$
7.0	$-6.8(3) \times 10^{-2}$	
10.0	$-3.79(18) \times 10^{-2}$	
15.0	$-1.81(6) \times 10^{-2}$	
20.0	$-9.4(3) \times 10^{-3}$	
40.0	$-2.41(9) \times 10^{-3}$	$-2.29(6) \times 10^{-3}$

B. Virial coefficients

Calculated values of B_8 are reported in Table I. For B_8, we achieved good precision for low and high temperatures. As shown in Fig. 1, it was difficult to obtain values with small relative uncertainty in the vicinity of the LJ critical temperature ($T \approx 1.3$). Comparison of the new values of B_8 with lower-precision data at a few temperatures reported by us previously[32] finds good mutual consistency.

Tables II and III report all coefficients computed here for B_9 to B_{16}. There are no literature data published before for values at these orders. As for B_8, we obtained values for B_9 with good precision at low and high temperatures and found difficulty getting good precision at intermediate temperatures. From B_{10} to B_{16}, we attempted calculation of coefficients only at low temperatures because it was increasingly difficult to get

TABLE II. Ninth to thirteenth virial coefficients of the Lennard-Jones model. All quantities given in LJ units.

T	B_9	B_{10}	B_{11}	B_{12}	B_{13}
0.6	$-9.75(11)\times10^{11}$	$-7.51(14)\times10^{13}$	$-6.31(9)\times10^{15}$	$-5.46(12)\times10^{17}$	$-5.18(13)\times10^{19}$
0.7	$-1.155(15)\times10^{10}$	$-4.89(9)\times10^{11}$	$-2.14(6)\times10^{13}$	$-9.3(5)\times10^{14}$	$-4.1(4)\times10^{16}$
0.8	$-3.00(6)\times10^{8}$	$-7.3(2)\times10^{9}$	$-2.05(15)\times10^{11}$		
0.9	$-1.18(5)\times10^{7}$	$-1.6(4)\times10^{8}$			
1.0	$-7.6(7)\times10^{5}$				
1.2	$-1.4(4)\times10^{4}$				
2.0	$-6(14)$				
3.0	$-1.4(6)$				
5.0	$-0.21(3)$				
10.0	$-3.3(3)\times10^{-2}$				
20.0	$-3.3(4)\times10^{-3}$				
40.0	$-4.6(7)\times10^{-4}$				

useful precision for the target system at intermediate and high temperatures.

Fig. 6 presents a plot of the coefficients as a function of N for several temperatures. The plot includes the values in Tables I, II, and III, and others that we obtained previously for the lower-order coefficients.[31,32] The dependence is clearly linear on this logarithmic scale, indicating an exponential increase in the magnitude of the coefficients with order.

For practical applications, it can be useful to have accurate expressions for the virial coefficients as a function of temperature. This allows the coefficients to be estimated for temperatures where MSMC data are not available, and it enables evaluation of temperature derivatives needed to compute quantities related to the thermodynamic energy and its derivatives. The development of an effective temperature-dependent form can be aided by a bit of analysis of Eqs. (2)-(5), which give B_N in terms of the LJ potential.

We start by separating the LJ form into its repulsive and attractive components, $u(r) = u_R(r) + u_A(r)$, for which $u_R(r) \equiv 4\epsilon_{\rm LJ}(r/\sigma_{\rm LJ})^{-12}$, and $u_A(r) \equiv -4\epsilon_{\rm LJ}(r/\sigma_{\rm LJ})^{-6}$. We then consider a separation of the Mayer function into corresponding repulsive and attractive components,

$$f = f_R + e_R f_A \equiv f_R + F, \tag{11}$$

where, using LJ units,

$$\begin{aligned} e_R &= e^{-(4/T)r^{-12}}, \\ f_R &= e_R - 1, \\ f_A &= e^{+(4/T)r^{-6}} - 1, \\ F &= e^{-(4/T)r^{-12}}\left(e^{+(4/T)r^{-6}} - 1\right). \end{aligned} \tag{12}$$

Now, turning to Eq. (3), we can rescale the integration variables, defining $s = (T/4)^{1/12}r$, and the equation then becomes

$$B_N = \left(\frac{T}{4}\right)^{-\frac{N-1}{4}} \frac{1-N}{N!} \int \cdots \int f_B(\mathbf{s}^N) d\mathbf{s}_{12} \ldots d\mathbf{s}_{1N}, \tag{13}$$

and in terms of the rescaled variables, Eq. (12) is

$$\begin{aligned} f_R &= \left(e^{-s^{-12}} - 1\right), \\ F &= e^{-s^{-12}}\left(e^{+(2/\sqrt{T})s^{-6}} - 1\right). \end{aligned} \tag{14}$$

In terms of the Mayer function decomposed as in Eq. (11), f_B is a sum of graphs, but with the usual f-bonds each replaced by either an f_R- or F-bond. Each graph in the original f-bond series for f_B is replaced by a sum of graphs having all such bond replacements. The F-bonds introduce temperature dependence to the scaled integral in Eq. (13). We can approximate the form of the temperature dependence introduced by each F-bond as $F \approx F_A \equiv \exp(A/\sqrt{T}) - 1$, where A is an adjustable constant (different for each N) that lumps the effect of integration over s. The temperature dependence of a graph having n F-bonds is thus estimated as F_A^n. We then sum over all graphs in f_B to get the full temperature dependence of B_N (in addition to the temperature-dependent prefactor). We note that in the limit $T \to \infty$, then $F \to 0$ while $B_N(T) \to B_N^{\rm SS}(T/4)$, where $B_N^{\rm SS}$ is the Nth virial coefficient for the soft-sphere model (with potential

TABLE III. Fourteenth to sixteenth virial coefficients of the Lennard-Jones model. All quantities given in LJ units.

T	B_{14}	B_{15}	B_{16}
0.6	$-4.9(3)\times10^{21}$	$-4.7(5)\times10^{23}$	$-4.5(9)\times10^{25}$
0.7	$-2.1(6)\times10^{18}$		

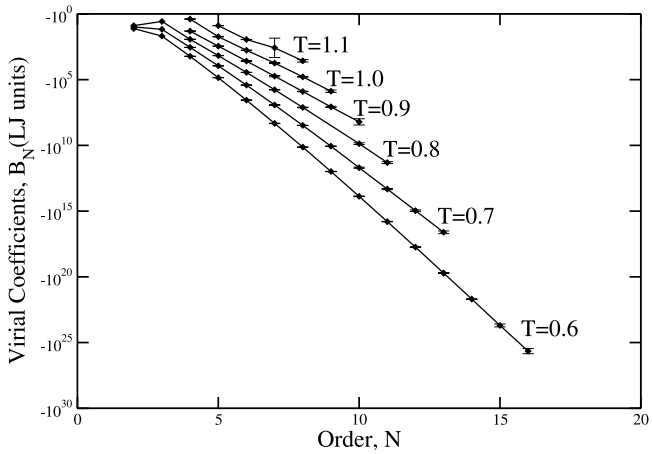

FIG. 6. Virial coefficients with increasing order at subcritical temperatures, as computed here ($N \geq 9$) and in previous work.[31,32]

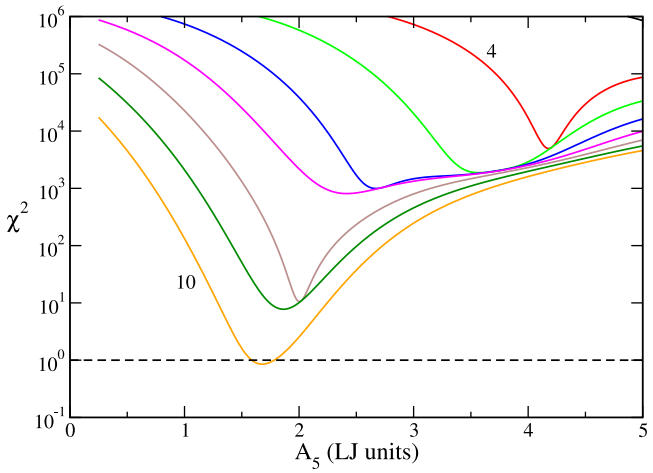

FIG. 7. Demonstration of fit of Eq. (15) for $N = 5$. Plotted is a reduced χ^2 statistic, defined as $n_N^{-1}\sum_i (B_{N,i} - B_N(T_i))^2/\sigma^2_{N,i}$, presented as a function of the nonlinear fitting parameter A_N. Each line shows the statistic for a different choice of k_N, the number of fitting constants, going in increments of 1 from $k_N = 4$ to 10, as indicated.

$u(r) = \epsilon_{LJ}(\sigma_{LJ}/r)^{12}$). Taken together, we have the following form for our fit of the virial coefficient B_N:

$$B_N(T) = \left(\frac{T}{4}\right)^{-\frac{N-1}{4}} \left[\bar{B}_N^{SS} + \sum_{k=1}^{k_N} a_{N,k}\left(e^{A_N/\sqrt{T}} - 1\right)^k\right], \quad (15)$$

where the $a_{N,k}$ (and A_N) are fitting parameters, and $\bar{B}_N^{SS}$ is the soft-sphere virial coefficient at unit temperature (equal to 3.527 61(6), 2.114 94(2), 0.769 53(4), 0.090 43(12), −0.0742(6), −0.035(3), for $N = 4$ (Ref. 40) and 5-9 (Ref. 17), respectively).

The sum in Eq. (15) extends to k_N, which is selected to provide sufficient values of k to form a good fit without overfitting the data. Fig. 7 illustrates the fitting process. Here, we plot the χ^2 statistic, reduced by n_N, which is the number of B_N values fit to Eq. (15). We reduce by this quantity instead of the degrees of freedom, $(n_N - k_N)$, because our aim is simply to quantify how well the fit describes the data to within their uncertainties, rather than assess the likelihood that the fit function is an exact description of the true $B_N(T)$ behavior (which we know it is not). This statistic is given in Fig. 7 as a function of the (non-linear) parameter A_N, with all other (linear) parameters $a_{N,k}$ determined by a weighted least-squares fit for the given A_N. For $\chi^2 > 1$, the function is not fitting the data to within their uncertainties, while $\chi^2 < 1$ represents an overfit of the data—the function matches the points better than is warranted by their uncertainties. We select k_N large enough to allow $\chi^2 \approx 1$ for some value of A_N, which we take as the best-fit value. An unnecessarily large k_N is indicated if $\chi^2 < 1$.

The parameters obtained by fitting each virial coefficient $B_N(T), 4 \le N \le 9$, are given in the supplementary material.[41] Fits for $N \ge 10$ were not attempted due to lack of data at intermediate and higher temperatures. For convenience, we also collect in the supplementary material[41] the best of the known values and uncertainties of all coefficients, $4 \le N \le 16$, in a machine-readable form. These data include a few new values for lower-order coefficients that were computed during the course of this work.

IV. CONCLUSION

We have applied the overlap-sampling implementation of Mayer sampling Monte Carlo and direct generation of configurations to evaluate high-order virial coefficients of the Lennard-Jones model, using Wheatley's algorithm for summation of clusters. We were able to obtain results up to $N = 16$, which is well beyond what was possible before these recent methodological advances. The focus of this study was on low temperatures, particularly for larger N, as that is where the calculations were most feasible. Such coefficients are of interest because they are at subcritical temperatures, so they may find use in advancing our understanding of condensation in the context of the virial equation of state.[42]

Based on current methods, it is still too expensive to explore coefficients of the LJ model at intermediate and high temperatures to obtain satisfactory precision for the orders above B_9. Such calculations must await further improvements to methodology and/or computer hardware, particularly in connection to massively parallel architectures, for which Monte Carlo methods, and MSMC, in particular, would be especially well suited if memory limitations can be overcome.

ACKNOWLEDGMENTS

Funding for this work was provided by a grant from U.S. National Science Foundation (NSF), Grant No. CHE-1027963. Computational resources were provided by the University at Buffalo Center for Computational Research.

[1]E. Mason and T. Spurling, *The Virial Equation of State* (Pergamon Press, Oxford, 1969).
[2]A. Bellemans, Physica **28**, 493 (1962).
[3]J. H. Yang, A. J. Schultz, J. R. Errington, and D. A. Kofke, J. Chem. Phys. **138**, 134706 (2013).
[4]J. H. Yang, A. J. Schultz, J. R. Errington, and D. A. Kofke, Mol. Phys. **113**, 1179 (2015).
[5]K. M. Benjamin, A. J. Schultz, and D. A. Kofke, J. Phys. Chem. B **113**, 7810 (2009).
[6]K. M. Benjamin, A. J. Schultz, and D. A. Kofke, J. Phys. Chem. C **111**, 16021 (2007).
[7]B. Jager, R. Hellmann, E. Bich, and E. Vogel, J. Chem. Phys. **135**, 084308 (2011).
[8]C. Joslin, Mol. Phys. **42**, 1507 (1980).
[9]G. Garberoglio and A. H. Harvey, J. Res. Natl. Inst. Stand. Technol. **114**, 249 (2009).
[10]G. Garberoglio and A. H. Harvey, J. Chem. Phys. **134**, 134106 (2011).
[11]K. R. S. Shaul, A. J. Schultz, and D. A. Kofke, J. Chem. Phys. **137**, 184101 (2012).
[12]A. J. Schultz, D. A. Kofke, and A. H. Harvey, "Molecular-based virial coefficients of CO_2-H_2O mixtures," AIChE J. (in press).
[13]M. Ushcats, Phys. Rev. Lett. **109**, 040601 (2012).
[14]M. V. Ushcats, J. Chem. Phys. **138**, 094309 (2013).
[15]M. V. Ushcats, J. Chem. Phys. **141**, 101103 (2014).
[16]A. J. Schultz and D. A. Kofke, J. Chem. Theory Comput. **10**, 5229 (2014).
[17]R. J. Wheatley, Phys. Rev. Lett. **110**, 200601 (2013).
[18]A. J. Schultz and D. A. Kofke, Phys. Rev. E **90**, 023301 (2014).
[19]J. Singh and D. Kofke, Phys. Rev. Lett. **92**, 22061 (2004).
[20]K. M. Benjamin, A. J. Schultz, and D. A. Kofke, Ind. Eng. Chem. Res. **45**, 5566 (2006).
[21]K. Benjamin, J. Singh, A. Schultz, and D. Kofke, J. Phys. Chem. B **111**, 11463 (2007).
[22]A. Schultz and D. Kofke, J. Chem. Phys. **133**, 104101 (2010).
[23]K. R. S. Shaul, A. J. Schultz, D. A. Kofke, and M. R. Moldover, Chem. Phys. Lett. **531**, 11 (2012).
[24]C. Zhang and B. M. Pettitt, Mol. Phys. **112**, 1427 (2014).
[25]K. R. S. Shaul, A. J. Schultz, and D. A. Kofke, Collect. Czech. Chem. Commun. **75**, 447 (2010).

[26]J. A. Barker, P. J. Leonard, and A. Pompe, J. Chem. Phys. **44**, 4206 (1966).
[27]D. Henderson and L. Oden, Mol. Phys. **10**, 405 (1966).
[28]S. Kim, D. Henderson, and L. Oden, Trans. Faraday Soc. **65**, 2308 (1969).
[29]T. Sun and A. S. Teja, J. Phys. Chem. **100**, 17365 (1996).
[30]K. M. Dyer, J. S. Perkyns, and B. M. Pettitt, Theor. Chem. Acc. **105**, 244 (2001).
[31]A. Schultz and D. Kofke, Mol. Phys. **107**, 2309 (2009).
[32]A. J. Schultz, N. S. Barlow, V. Chaudhary, and D. A. Kofke, Mol. Phys. **111**, 535 (2013).
[33]C. Feng, A. Schultz, V. Chaudhary, and D. Kofke, in IEEE International Conference on High Performance Computing, Goa, India, 2014, p. 1.
[34]D. McQuarrie, *Statistical Mechanics* (Harper & Row, New York, 1976).
[35]D. A. Kofke, Fluid Phase Equilib. **228-229**, 41 (2005).
[36]C. H. Bennett, J. Comput. Phys. **22**, 245 (1976).
[37]D. Frenkel and B. Smit, *Understanding Molecular Simulations: From Algorithms to Applications* (Academic Press, San Diego, 2002).
[38]F. H. Ree and W. G. Hoover, J. Chem. Phys. **40**, 939 (1964).
[39]M. Matsumoto and T. Nishimura, ACM Trans. Model. Comput. Simul. **8**, 3 (1998).
[40]T. B. Tan, A. J. Schultz, and D. A. Kofke, Mol. Phys. **109**, 123 (2011).
[41]See supplementary material at http://dx.doi.org/10.1063/1.4927339 for a list of all known virial coefficients B_N, $4 \le N \le 16$, for the Lennard-Jones model, and parameters for the virial-coefficient fits reported in this work.
[42]A. J. Schultz and D. A. Kofke, "Virial equation of state of the Lennard-Jones fluid using extrapolated high-order coefficients," Fluid Phase Equilib. (submitted).